Simulation of strong ground motions caused by the 2004 off the Kii peninsula earthquakes

Toshihiko Hayakawa, Takashi Furumura, and Yoshiko Yamanaka

Earthquake Research Institute, University of Tokyo 1-1-1 Yayoi, Bunkyo-ku, Tokyo 113-0032, Japan

(Received November 30, 2004; Revised February 28, 2005; Accepted March 1, 2005)

Strong ground motions caused by the Mj 7.4 2004 earthquake that occurred in the Nankai Trough to the southeast of the Kii Peninsula, Japan are simulated by a three-dimensional (3D) finite-difference method (FDM) using a fault-rupture model obtained by inversion of teleseismic seismograms and a 3D subsurface structure model for central Japan. Through simulations of the foreshock (Mj 7.1), the structural model is refined by comparison with observations, and the modified model is used to simulate the mainshock. The simulation provides a reasonable reproduction of the ground motions caused by the mainshock, including site amplification effects in the sedimentary basins of Osaka and Noubi. However, the current simulation model has limitations in producing the large and extended ground motion due to long-period Love waves in the Kanto Plain, as the model does not account for the sharp frequency selectivity for Love waves in the surficial structure of the Bouso Peninsula. It therefore appears necessary to develop a better model for longer-period waves.

Key words: Strong motion, simulation, FDM, 3D structure.

1. Introduction

A large Mj 7.4 earthquake occurred in the Nankai trough to the southeast of the Kii Peninsula on 5 September 2004 at 23:57 Japan Standard Time (JST) (Fig. 1). The source mechanism of this earthquake has been determined by the Japan Meteorological Agency (JMA) to be a thrust-fault event in the subducting Philippine Sea Plate at a depth of about 38 km. Although this earthquake did not cause severe damage, it deserves considerable attention as it produced large and extended ground shaking in the nearest population centers several hundred kilometers from the hypocenter. As large M8 earthquakes have repeatedly occurred in the Nankai trough at an almost uniform recurrence interval of approximately 100 yr, and because the area is conspicuously inactive between these major events, the observations of this most recent earthquake offer a valuable opportunity to gain a better understanding of the strong ground motions expected for future Nankai Trough earthquakes.

A notable feature of the 2004 earthquake was that long-period ground motions of 2–10 s or longer were observed in major population centers such as Osaka, Nagoya, and Tokyo, sites located on large sedimentary basins. This is the first such event to have occurred since the deployment of the dense, nationwide strong motion instruments (K-NET and KiK-net) across Japan in 1996. Although the maximum intensity in Tokyo was quite low (4 on the JMA 7-point scale), high ground velocities of over 5 cm/s were experienced in the center of Tokyo and on the Bouso Peninsula. These velocities are several times higher than that expected from the empirical attenuation function (e.g., Shi and Midorikawa, 1999) for an M7.4 event.

Considerable attention has been paid to the threat of long-period ground motions to large-scale constructions since the Tokachi-oki (Mj 8.0) earthquake of 26 September 2003. Oil reserve tanks at Tomakomai suffered significant damage due to the motion of strong long-period signals propagating distances of over 200 km from the source. Structural engineering studies revealed that the damage to these oil tanks was caused by the violent motion of the floating roof due to resonance at the long-period ground shaking period of 7 s (Hatayama and Zama, 2004).

The subsurface structure of the Kanto Plain is very complex, with thick (>4000 m) sediments overlying rigid bedrock. Long-period surface waves (Love waves) with periods of 5–10 s or longer are commonly generated at the basin edge (e.g., Koketsu and Kikuchi, 2000). Thus, detailed understanding of wave propagation from a hypocenter to the basin of Tokyo and the characteristics of surface wave generation in the thick sedimentary basin is very important for mitigation of potential damage at population centers expected to be affected by future damaging earthquakes such as those that occur in the Nankai Trough.

The present study validates the subsurface structural model for central Japan, derived recently based on a number of geophysical surveys, by comparison of the observed seismograms with model simulations. Simulations of the foreshock are compared with observed waveforms assuming a source-slip model, and the structural model is refined to achieve a better reproduction of observations. Using this modified model with a source-slip model for the earthquake (Yamanaka, 2004), the ground motions caused by the mainshock are simulated.

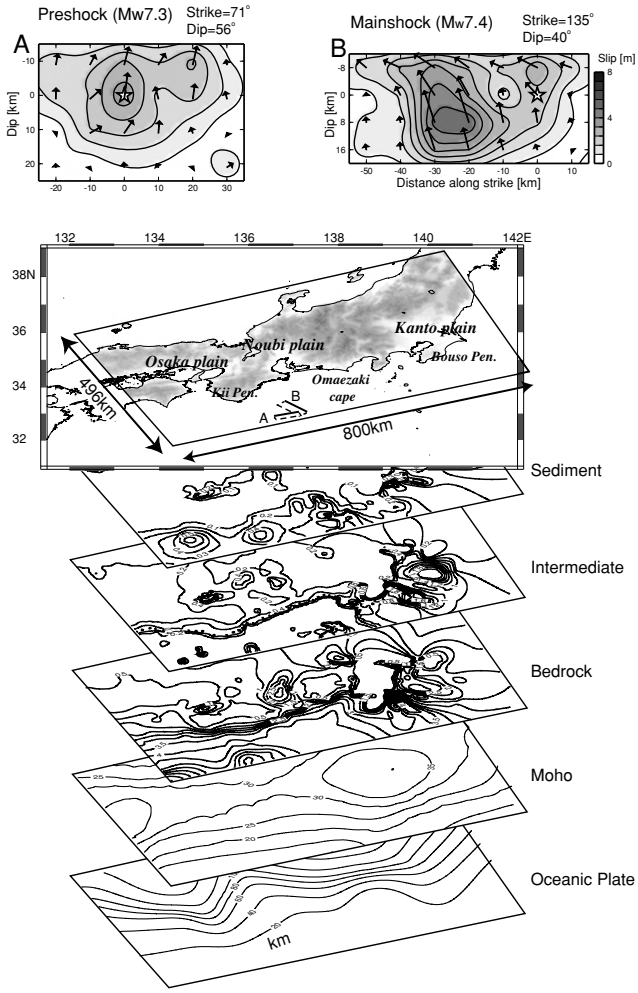

Fig. 1. Source-slip model and 3D velocity structure model used for simulation. White stars denote rupture-starting points, and contours represent the depth of each layer.

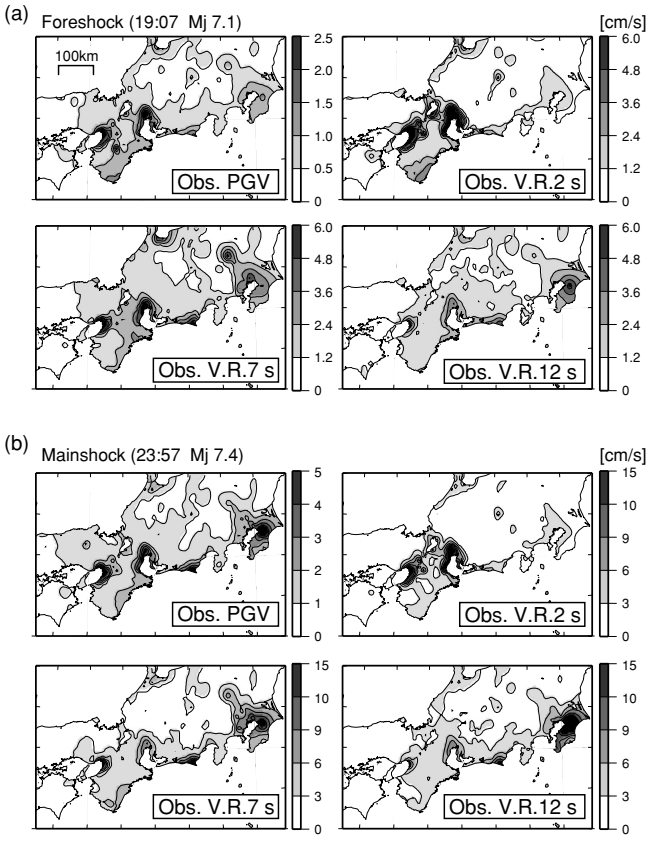

Fig. 2. Observed and simulated PGV and VR distributions for horizontal motion with periods of 2, 7, and 12 s. (a) Foreshock, (b) mainshock. PGV values were calculated using filtered waveform at a high-cut frequency of 0.5 Hz.

2. Observations of Ground Motion

Figure 2(a) shows the pattern of ground motions associated with the foreshock (19:07, Mj 7.1) of the earthquake off the Kii Peninsula. The distributions of peak ground velocity (PGV) motions and the pseudo-velocity response (VR) of 5% dumping at periods of 2, 7, and 12 s are shown in the figure. A large data set of responses from over 800 accelerometers of the K-NET, and Kik-net seismic networks was used to evaluate the attenuation characteristics and localized amplification effects at population centers. The PGV displays a complex distribution with a number of localized peaks in sedimentary basins, such as in the Kanto, Noubi and Osaka plains. A high VR of over 6 cm/s can be seen to have occurred in Osaka and Noubi at a period of 2 s. In the center of Kanto Plain, even higher velocity responses were detected, and with a much longer period of over 7 s. Furthermore, the eastern part of the Kanto Plain is marked by VR exceeding 3 cm/s at a period of 12 s. The longer dominant period of the VR in the Kanto basin is related to the presence of thick sediments of 3000–4000 m in thickness overlying rigid bedrock. The lower resonant period (2 s) observed for the Noubi and Osaka plains is thus considered to reflect the thinner sediments (<2000 m) of those basins.

The PGV and VR distributions for the main shock (23:57, Mj 7.4) event are shown in Fig. 2(b) using a magnified color scale. The pattern for the mainshock event is very similar to that for the foreshock event (Fig. 2(a)) except for the Bouso Peninsula. Ground shaking of over 5 cm was detected in Tokyo and on the Bouso Peninsula during the mainshock event due to the resonance of long-period signals with a period of longer than 7 s. However, no such large responses were observed in Tokyo or on the Bouso Peninsula during the foreshock event (Fig. 2(a)), even though both earthquakes have similar source locations and mechanisms. Thus, the discrepancy between these PGV and VR can be attributed primarily to the differences in the magnitudes of these events, i.e. the larger magnitude source radiates waves with significantly longer periods than the small event.

Comparison between the waveforms recorded by the Kik-net station on the Bouso Peninsula (CHBH10) for the mainshock and foreshock events reveal the difference in the source spectrum and amplification characteristics of long-period signals in Tokyo during the small (Mj 7.1) and large (Mj 7.4) events (Fig. 3). The generation of long-period signals during the mainshock event can be confirmed from the transverse seismograms and particle motions, thus allowing the Love wave to be identified. However, no such large and extended Love-wave train can be seen in the waveform of

Table 1. Physical parameters for each layer of the 3D model.

Layer	Depth [km]	Vp [m/s]	Vs [m/s]	Density [kg/m^3]	Qp	Qs
Surficial Layer (Initial)						
Sediment	0–0.8	1800	500	1900	90	60
Intermediate	0–3	2400	1000	2100	150	100
Bedrock	0–7.2	3200	1700	2700	225	150
Surficial Layer (Modified)						
Sediment 1	0–0.5	1800	500	1900	90	60
Sediment 2	0–0.7	2100	700	2000	150	100
Intermediate	0–3	3100	1400	2300	150	100
Bedrock	0–7.2	4000	2000	2700	225	150
Basement (Common)						
Upper crust	4.2–16.8	6000	3600	2700	450	300
Lower crust	10–40	6600	3700	2700	600	400
Mantle	40–70	7800	4200	3200	750	500
Slab	1–170	8100	4680	3300	2250	1500

the foreshock (Mj 7.1) event, even though the early-arrival direct *S* waves have almost the same waveform. The velocity response for the foreshock and mainshock record cannot be compared directly because of different duration recordings, though the amplification of waves longer than 4 s is found only for the mainshock event.

3. Numerical Simulation

Simulations of ground motions for the foreshock of the 2004 event off the Kii Peninsula were conducted to evaluate the wave propagation characteristics in the heterogeneous crust and upper mantle structure of central Japan. A parallel, multi-grid finite-difference method (FDM) was employed (Furumura and Chen, 2004, 2005) for simulation of the seismic wavefield in the 3D heterogeneous structure. For concurrent computing using a large number of processors, the 3D model was divided vertically into subdomains for assignment to parallel processors. Shallow basin structures were incorporated into the large 3D model using a multi-grid approach to embed a finer mesh model upon the coarse mesh body. A 16th-order staggered-grid FDM was adopted for calculation of derivatives in the equations of motion in the horizontal direction, and a conventional fourth-order staggered-grid FDM was used in the vertical direction. Anelastic attenuation (Q) of the seismic wavefield was implemented using the viscoelastic technique of Blanch *et al.* (1995), which offers frequency-independent attenuation characteristics for *P* and *S* waves (Qp and Qs) over a wide frequency range. To suppress artificial reflections at the outer limits of the volume, we introduce 20-node absorbing zones (Cerjan *et al.*, 1985) and the nonreflecting boundary condition of Clayton and Engquist (1977). The zero-stress boundary conditions at surface of Graves (1996) are also applied. The simulation model covers an area of 800 km by 496 km and extends to a depth of 141 km. The volume is discretized using a grid size of 0.8 km in the horizontal direction, and 0.4 km in the vertical direction for the major part of the model, and a smaller grid size of 0.4 km in the horizontal direction, and 0.2 km in the vertical direction is defined for depths shallower than 6 km.

The structural model and physical parameters of each

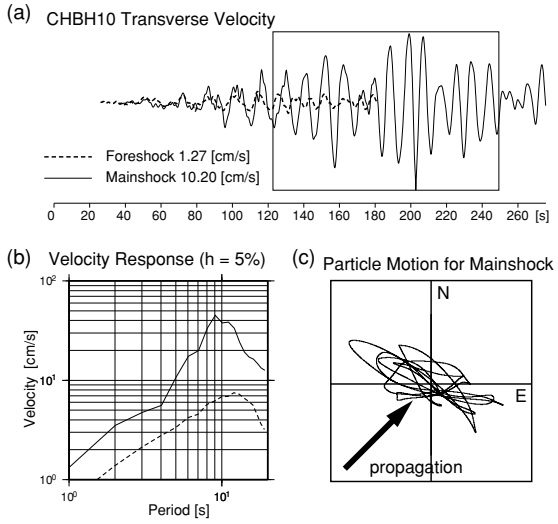

Fig. 3. (a) Ground motion at CHBH10, in the center of the Bouso Peninsula. (b) VR spectra with 5% damping for the mainshock (solid) and foreshock (dashed). (c) Particle motion of late-arrival waves (hatched area in (a)).

layer of the 3D model were constructed based on datasets obtained by recent refraction and reflection surveys, microtremor experiments, and borehole investigations (Central Disaster Management Council of Japan; CDMCJ, 2002), as shown in Fig. 1 and Table 1. The depth distribution of the Moho discontinuity was introduced in the simulation model based on the study of Ryoki (1999) using gravity anomaly data. The depth of the mid-crustal (Conrad) interface was assumed to lie midway between the free surface and the Moho boundary. The depth distribution of the top layer of the Philippine Sea Plate was derived from Yamazaki and Ooida (1985) using a hypocenter of microseisms (Fig. 1), and the oceanic crust and oceanic mantle for the plate are assumed to be 5 and 20 km thick, respectively.

A detailed subsurface structural model for the Kanto basin has recently been investigated by Yamanaka and Yamada (2002) using a large data set compiled from reflection

and refraction experiments, deep borehole data, and array analysis of microtremors. The structure of the sedimentary layers of the Kanto basin was constructed as a three-layer model with velocities of $Vs = 0.5$, 1.0 and 1.7 km/s. The three-layer basement model for the Kanto basin was connected to the nationwide structural model of CDMCJ by connecting the interfaces of these sedimentary layers to the 2nd, 3rd and 4th layer of the nation-wide structure model.

The source-slip model used here was derived from an inversion of teleseismic waveforms recorded by the IRIS-DMC broadband network (Yamanaka, 2004). The size of the fault was set at 60 × 24 km, and was represented by point slips distributed at intervals of 2 km, each slip of 2 s is associated with the passage of a rupture front at an average speed of 2.5 km/s. The source slip function at each subfault was described as a triangle function with a 1 s rise and 1 s falloff.

Using 16th-order staggered FDM, the seismic wave propagation at frequency limit 0.5 Hz can be calculated at a resolution of three grid samples per shortest wavelength with a grid dispersion error of less than 1%. In addition, the fourth order staggered FDM used in vertical direction requires five grid samples per shortest wavelength. To achieve the some accuracy the time sampling interval is 0.01 s, which was derived from stability criterion of FDM operator (Levander, 1988). The parallel simulation was conducted using the Earth Simulator supercomputer at the Japan Marine Science and Technology Center (JAMSTEC). Computation required 60 Gbyte of memory and a wall-clock time of 30 h using 8 nodes (64 processors) of the Earth Simulator.

4. Simulation Results

4.1 The foreshock

The results of the FDM simulation for the foreshock of the Kii Peninsula earthquake are shown in Fig. 4(a). The figure shows the PGV and VR distributions for horizontal motions at periods of 2, 7 and 12 s for comparison with observations shown in Fig. 2(a).

The larger amplification of ground motions in such sedimentary basins such as the Noubi Plain at periods of 2 s is well reproduced by the simulations. However, at longer periods of 7 or 12 s, the VR values in these basins are several times larger than the observed values. A comparison of the synthetic and observed radial-component seismograms (Fig. 4(c)) shows a strong Rayleigh wave (underlined in the figure), which is considered to have developed in the low velocity surficial layer below GIFH29 and WKYH07. By examining different physical parameters of the structure model, this disagreement was interpreted as being due to the thickness and seismic speed employed for the surficial layer, both of which appear to be overestimated. Thus, the first ($Vs = 0.5$ km/s) surficial layer was divided into two layers of $Vs = 0.5$ and 0.7 km/s, and the velocity of the other crustal layers were adjusted, as shown in Table 1. The results of the simulation using the revised velocity model are shown in Fig. 4(b), demonstrating good improvements in the accuracy of the simulation. As the upper-most layer is now thinner, the amplitude of surface waves excited in the Noubi Basin has been reduced and is now consistent with the observations, accurately reproducing the VR at 7 s (Fig. 4(c); GIFH29). The overestimation of VR at 7 and 12 s in the western part of the Kii Peninsula and Shikoku Island have also been improved due to the lower velocity contrast between the surficial layer and bedrock (Fig. 4(c); WKYH07). Other stations at bedrock sites, such as SZOH43, remain largely unchanged by this modification of the surficial layer structure.

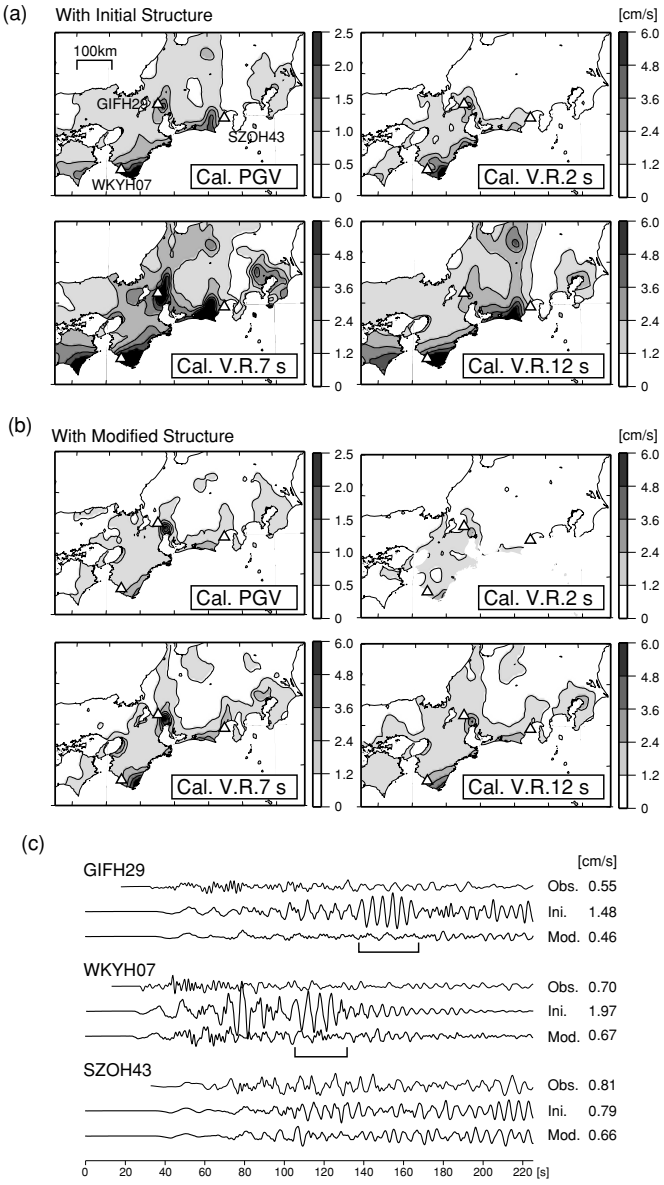

Fig. 4. Simulated PGV and VR distribution at periods of 2, 7, and 12 s for horizontal motion caused by the foreshock using (a) the initial 3D structural model, and (b) the modified model. (c) Comparison of radial waveforms at GIFH29, WKYH07, and SZOH43: observed (upper trace), simulation using the initial model (middle trace), and simulation using the modified model (lower trace). Trace amplitude is shown to the right. A portion of the wave identified as a Rayleigh wave is underlined.

4.2 The mainshock

A simulation of seismic wave propagation for the mainshock of the earthquake off the Kii Peninsula (Mj 7.4) was subsequently conducted using the modified structural model described above. Figure 5 shows a sequence of snapshots of horizontal ground velocity motion at 45, 70, 110, and 220 s following the start of the source rupture. In the

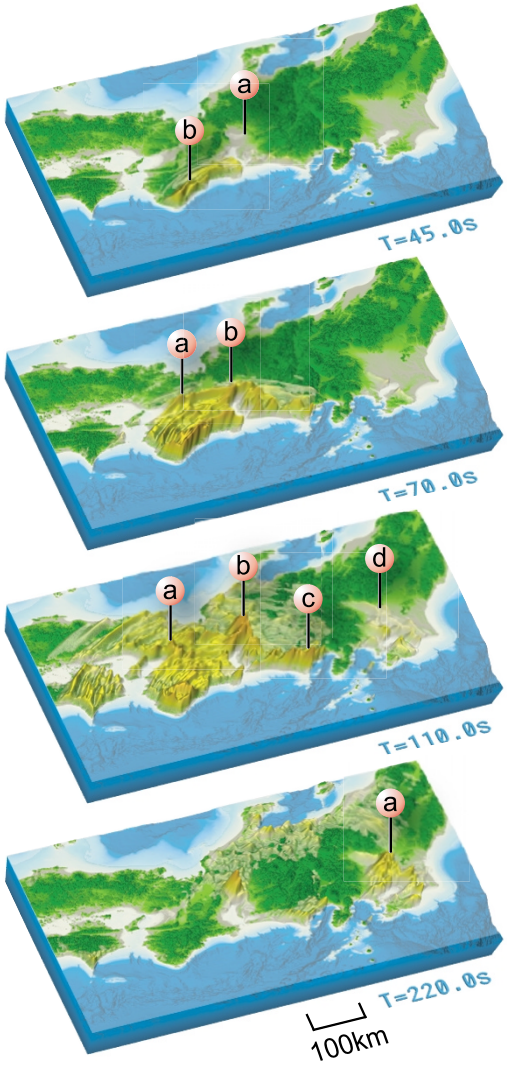

Fig. 5. Snapshots of simulated ground motion caused by the mainshock of the earthquake off the Kii Peninsula. Elapse times from fault rupture initiation are shown at the bottom right. Major phases are marked.

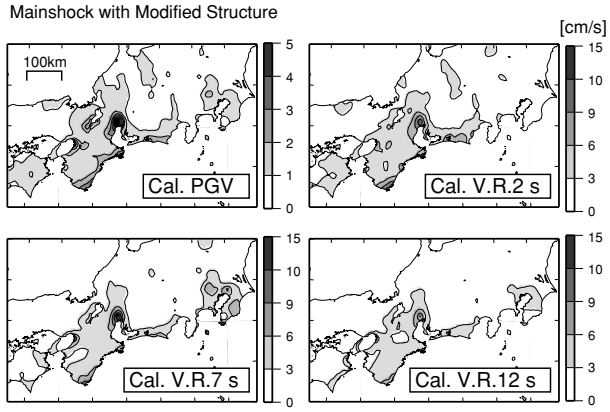

Fig. 6. Simulated PGV and VR distribution at periods of 2, 7, and 12 s for horizontal motion caused by the mainshock event.

first frame (45 s), the first arrival of *P* waves can be seen as a small anomaly on the Noubi Plain (45 s, mark 'a'). Due to the effect of rupture directivity at the fault, larger *S* waves are radiated to the east, emphasizing the large ground motion along the coastline of the Kii Peninsula (45 s, 'b'). As the *S* wave emerges on the Osaka Plain at 70 s, large surface waves are induced by the conversion of *S* waves at the basin edge (70 s, 'a'). Very large surface waves, several times larger than that in Osaka, occur in the Noubi Plain at a similar time due to excitation by the local deep structure (70 s, 'b'). Ground shaking in these basins is sustained for more than 110 s after the main *S*-wave signal has left the basins (110 s, 'a' and 'b').

Larger ground motions also emerge at the Cape of Omaezaki, where the speed of surface-wave propagation tends to decrease due to the subducting descent of bedrock at 2 km (110 s, 'c'). This effect is augmented by the long-period waves generated in the Nankai trough and constructive interference between the two waveforms, resulting in large ground motion for an extended period at Omaezaki.

The excitation of Love waves at the western edge of the Kanto Plain is pronounced in the last two frames, and large-amplitude ground motions can be seen to propagate across the Kanto Plain from west to east at wave speeds slower than 1 km/s (110 s, 'd' and 220 s, 'a'). From analysis of the three-component seismograms, the larger signals are considered to represent the fundamental-mode Love waves generated by multiple SH-wave reflections in the low-velocity layer at the basin edge.

The PGV and VR pattern (Fig. 6) produced by the simulation agrees well with the observations (Fig. 2(b)). Larger VR values for periods of 2 and 7 s appear in major sedimentary basins such as Osaka, Noubi, and Omaezaki, which is consistent with observations. However, the large VR values at a longer period of 12 s in the Kanto region, as observed during the mainshock of the Kii Peninsula earthquake, are not clearly reproduced in the simulation results. This disagreement was not observed in the previous simulations of the foreshock event, suggesting that the discrepancy may be due to the incompleteness of the structural model below Tokyo with respect to the propagation of long-period waves longer than 7 s. It therefore appears necessary to develop a better model for longer-period waves.

Synthetic seismograms of radial- and transverse-component ground velocities are illustrated in Fig. 7 along with the observed ground motions for comparison (high-cut record). The figure confirms good agreement between the simulation and observations in terms of the amplitude and duration of ground motions from the beginning of the direct *S* wave incidence to the *S*-wave coda. However, the large ground shaking of the particularly transverse component with periods of 10 s or more observed at CHBH10 is not clearly reproduced by the current simulation. The seismogram is well reconstructed on the western edge of the Kanto plain (TKYH12), whereas the matching is not good in front of the Izu Peninsula (SZO018). These behaviors suggest the disagreements at CHBH10 and SZO018 are mainly caused by the deep sediment structures.

5. Conclusion

The prediction of strong ground motions, including long-period waves and high-frequency signals for future earthquake scenarios, is very important for the mitigation of

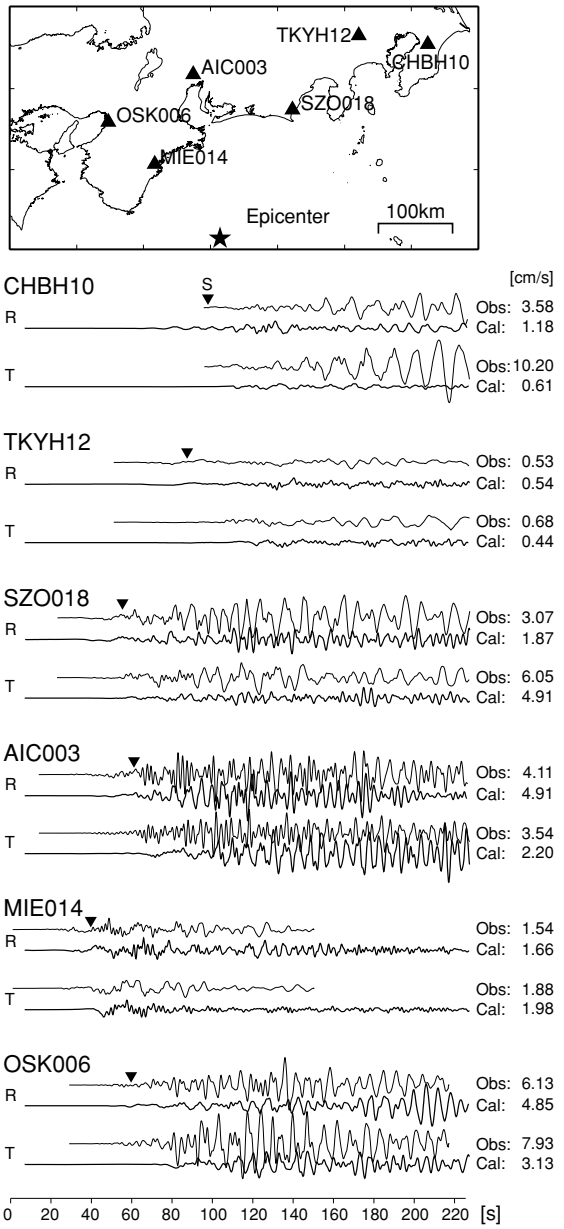

Fig. 7. Simulated and observed waveforms of radial and transverse ground velocities at six stations (CHBH10, TKYH12, SZO018, AIC003, MIE014, and OSK006). Trace amplitude is shown to the right.

earthquake disasters, and accurate prediction requires a good understanding of seismic wave propagation through 3D heterogeneous structures along the wave propagation path from the source. The simulations of wave propagation and strong ground motions for the 2004 off the Kii Peninsula earthquake conducted in this study were performed using a fault-rupture model obtained by inversion of teleseismic seismograms and a detailed 3D subsurface structure model for central Japan. The structural model was improved by matching the simulation to observations using a simple source model for the foreshock event.

The simulation of the mainshock reproduces the observed ground motions well, although the large ground shaking in the Kanto basin, characterized by a long-period motion of greater than 7 s, could not be reproduced accurately. Miyake and Koketsu (2005) inferred that not only the deep sediments but also the low-velocity surface layers developed the basin surface waves. On the other hand, Hara (2005) suggested the mainshock consisted of two different source mechanisms. With further refinement of the deep and surficial structural model for the propagation of the longer-period signals and the use of more reliable source models, it is hoped that future simulations will more closely reproduce the observations, particularly for damaging, long-period motions.

Acknowledgments. Computations were carried out on the Earth Simulator (JAMSTEC) under the research project entitled "Seismic wave propagation and strong ground motions in 3D heterogeneous structure" in 2004. Figures were prepared using GMT (P. Wessel and W. H. F. Smith). Constructive comments from Profs. H.-W. Chen and K. Yomogida, and an anonymous reviewer are greatly appreciated to improve the manuscript.

References

Blanch, J. O, J. O. A. Robertson, and W. W. Symes, Modeling of a constant Q: Methodology and algorithm for an efficient and optimally inexpensive viscoelastic technique, *Geophysics*, **60**, 176–184, 1995.

Central Disaster Management Council of Japan, Report for the Expert Committees about Tonankai and Nankai Earthquake, 2002. (http://www.bousai.go.jp/jishin/chubou/nankai/5/index.html)

Cerjan, C. D., D. Kosloff, R. Kosloff, and M. Reshef, A nonreflecting boundary condition for discrete acoustic and elastic wave equations, *Geophysics*, **50**, 705–708, 1985.

Clayton, R. W. and B. Engquist, Absorbing boundary conditions for acoustic and elastic wave equations, *Bull. Seism. Soc. Am.*, **67**, 1529–1540, 1977.

Furumura, T. and L. Chen, Large scale parallel simulation and visualization of 3D seismic wavefield using the Earth Simulator, *CMES*, **6**, 153–168, 2004.

Furumura, T. and L. Chen, Parallel simulation of strong ground motions during recent and historical damaging earthquakes in Tokyo, Japan, *Parallel Computing*, 2005.

Graves, R. W., Simulating seismic wave propagation in 3D elastic media using staggered-grid finite differences, *Bull. Seism. Soc. Am.*, **86**, 1091–1106, 1996.

Hara, T., Change of the source mechanism of the main shock of the 2004 off the Kii peninsula earthquakes inferred from long period body wave data, *Earth Planets Space*, **57**, this issue, 179–183, 2005.

Hatayama, K. and S. Zama, Characteristics of long-period ground motion during the Tokachi-oki, Japan, Earthquake in 2003, *Rep. Natl. Res. Inst. Fire Disast.*, **97**, 15–25, 2004.

Koketsu, K. and M. Kikuchi, Propagation of seismic ground motion in the Kanto basin, Japan, *Science*, **288**, 19, 1237–1239, 2000.

Levander, A. R., Fourth-order finite-difference P-SV seismograms, *Geophysics*, **64**, 1425–1436, 1988.

Miyake, H. and K. Koketsu, Long-period ground motions from a large offshore earthquake: The case of the 2004 off the Kii peninsula earthquake, Japan, *Earth Planets Space*, **57**, this issue, 203–207, 2005.

Ryoki, K., Three-dimensional depth structure of the crust and uppermost mantle beneath Southwestern Japan and its regional gravity anomalies, *Zisin 2*, **52**, 51–63, 1999.

Si, H. and S. Midorikawa, New attenuation relationships for peak ground acceleration and velocity considering effects of fault type and site condition, *J. Struct. Constr. Eng.*, **523**, 63–70, 1999.

Yamanaka, H. and N. Yamada, Estimation of 3D S-wave velocity model of deep sedimentary layers in Kanto-plain, Japan, using microtremor array measurements, *Butsuri-Tansa*, **55**, 53–65, 2002.

Yamanaka, Y., EIC Seismological note: No. 153, 2004 (http://www.eri.u-tokyo.ac.jp/sanchu/Seismo_Note/2004/EIC153.html)

Yamazaki, F. and T. Ooida, Configuration of subducted Philippine sea plate beneath the Chubu distinct, central Japan, *Zisin 2*, **38**, 193–202, 1985.

T. Hayakawa (e-mail: t-haya@eri.u-tokyo.ac.jp), T. Furumura, and Y. Yamanaka